Effect of Electric Field on the Exchange-Stiffness Constant in a $Co_{12}Fe_{72}B_{16}$ Disk-Shaped Nanomagnet 65 nm in Diameter

Jaehun Cho,[1,*] Shinji Miwa,[1,2] Kay Yakushiji,[3] Hitoshi Kubota,[3] Akio Fukushima,[3] Chun-Yeol You,[4,5] Shinji Yuasa,[3] and Yoshishige Suzuki[1,2,3,6]

[1]*Department of Materials Engineering Science, Osaka University, Toyonaka, Osaka 560-8531, Japan*
[2]*Center for Spintronics Research Network (CSRN), Toyonaka, Osaka 560-8531, Japan*
[3]*AIST, Spintronics Research Center, Tsukuba, Ibaraki 305-8568, Japan*
[4]*Department of Emerging Materials Science, DGIST, Daegu 42988, South Korea*
[5]*Global Center for Bio-Convergence Spin System, DGIST, Daegu 42988, South Korea*
[6]*MI²I, National Institute for Material Science, Japan*

(Received 05 July 2017; revised manuscript received 22 January 2018; published 30 July 2018)

The exchange stiffness constant denoted by A_{ex} is one of the fundamental physical quantities from the Heisenberg exchange Hamiltonian for ferromagnetic materials. A recent theoretical prediction shows the possibility that A_{ex} in ferromagnetic metal films can be effectively tuned by the application of an electric field at the surface. In this paper, we demonstrate that the thermally excited spin-wave modes in magnetic tunnel junctions contain modulations upon application of an electric field through a MgO tunneling barrier. Different modulations of different spin-wave eigenmodes provide quantitative information regarding the electric field effects on the exchange stiffness, perpendicular anisotropy energy, and saturation magnetization. An electric field of 1 V/nm modulated A_{ex} by 8.1% at room temperature. The results are significantly higher than those predicted from the Slater-Pauling curve and recent theoretical work.

DOI: 10.1103/PhysRevApplied.10.014033

I. INTRODUCTION

The electric field control of the magnetic properties in metallic ferromagnets has attracted considerable attention owing to its potential as a key technology in the production of ultralow-energy-consumption spintronic devices. The electric field control of magnetic anisotropy in a ferromagnetic metal system at room temperature [1,2] is of particular interest for ultralow-power magnetic random access memory (MRAM) applications [3–10]. Furthermore, Chiba *et al.* reported a significant electric field effect on the Curie temperature T_C, in Co ultrathin films [11]. Oba *et al.* theoretically predicted the electric field control of the Heisenberg exchange constant in a ferromagnetic layer without capping layer (i.e., ferromagnetic metal in the vacuum) [12]. This theory successfully describes the electric field dependence on T_C. However, two groups have recently reported the electric field control on maze domain size [13,14] that is determined by the minimizations of the total system energy, including the exchange, perpendicular magnetic anisotropy, and dipole interaction energies. These two studies provided different conclusions from analyses of experimental observations; the estimated change in the exchange stiffness constant, A_{ex}, differs in magnitude and sign for each study, although similar magnetic systems were employed, i.e., Co and Co-Fe-B. Therefore, the electric field control of the exchange interaction in 3*d* ferromagnets must be addressed with more consideration of the experimental technique and analysis. With the appropriate modeling, the contribution of the change in A_{ex} could be separated from those of the perpendicular magnetic anisotropy and saturation magnetization. The electric field control of A_{ex} may provide the additional functionality for magnetic materials, such as the electric field switching of ferromagnetism [4], creation and annihilation of skyrmions (working together with the electric field control of the Dzyaloshinskii-Moriya interaction [15,16]), control of the magnon velocity, and T_C [11]. For example, the electric field control of the skyrmion has already been demonstrated under an STM tip [17] and in a junction [18]. However, in these experiments, the quantitative information regarding the modulation in A_{ex} is lacking. Therefore, a quantitative evaluation technique is required for the exchange interaction in ferromagnetic films under electric field applications based on an independent experimental approach.

In our previous research, the spin-wave eigenmodes on a 2-nm-thick FeB free layer with 120–300-nm-diameter magnetic tunnel junctions (MTJs) with perpendicular magnetization were classified with various nodal circles (n) modes and nodal diameter (l) modes [19,20]. The

*cho@spin.mp.es.osaka-u.ac.jp

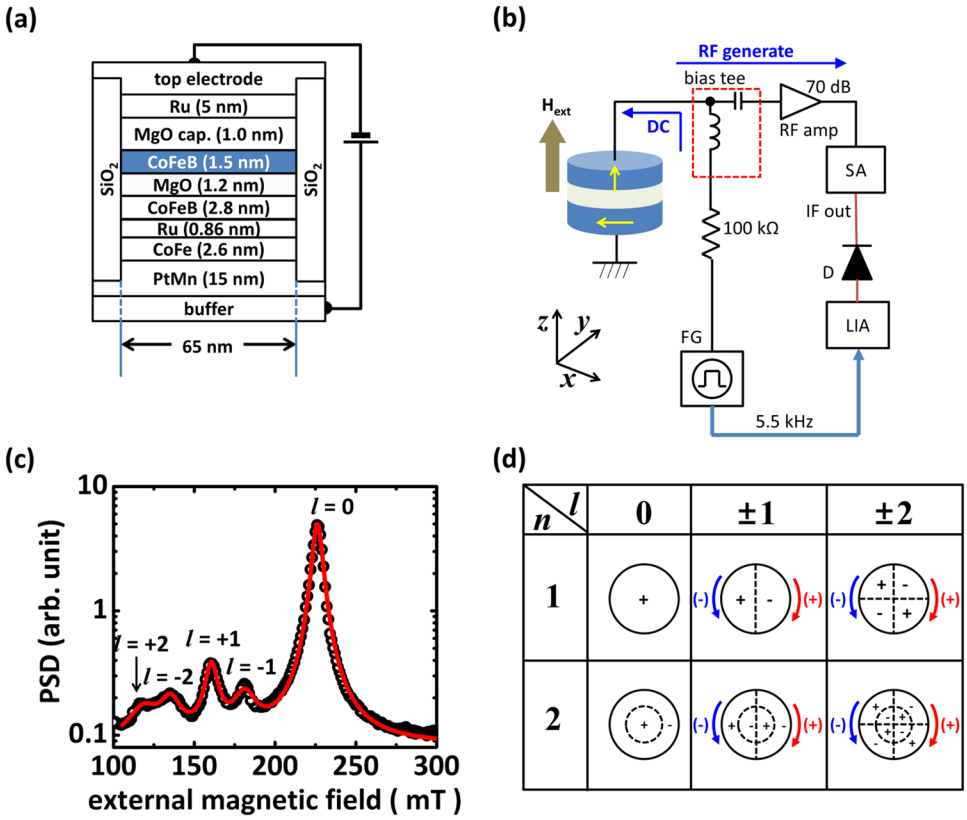

FIG. 1. (a) Schematic of the device structure. (b) Schematic configuration of the measurement circuit. SA, D, LIA, and FG stand for the spectrum analyzer, negative diode detector, lock-in amplifier, and function generator, respectively. (c) Field-sweep noise measurement spectrum at 6.0 GHz under a bias of 0.52 V. The open black circles represent the experimental data and the red solid line is the Lorentzian fit result. All modes correspond to the nodal circle $n = 1$ mode. The indices of the nodal diameter modes are shown in the graph. (d) Schematic diagram of the wave function in each nodal mode.

fundamental uniform resonance frequency of the cell [similar to the ferromagnetic resonance (FMR) mode with a zero spin-wave vector] is mostly determined by the saturation magnetization (M_s), perpendicular magnetic uniaxial anisotropy, and external magnetic field (H_{ext}). In the experimental spectrum, additional higher nodal modes appear with a finite nonzero spinwave vector and the splitting between different nodal modes is determined primarily by A_{ex}, as a non collinear spin configuration is required within a nanostructure. Conversely, the splitting between modes with different propagation directions (directional splitting between $\pm l$ modes) is caused by dipole coupling that is governed by the size of M_s. The characteristic appearance of M_s, A_{ex}, and perpendicular magnetic uniaxial anisotropy in the mode frequency splitting provides an effective method to selectively analyze the electric field effect on A_{ex}.

In this study, a 65-nm-diameter MTJ with perpendicular magnetic anisotropy was prepared by electron-beam lithography to investigate the electric field modulation of A_{ex}. In smaller samples, higher nodal modes require a large wave number k, providing larger exchange splitting, and are sensitive to small changes in A_{ex}. The thermally excited ferromagnetic resonance (TE FMR) measurements were employed to measure the electric field effect on the spin-wave eigenmodes in the free layer of the MTJ. Using the electric field dependence of the higher-mode spin-wave spectra, each contribution of A_{ex}, M_s, and perpendicular magnetic anisotropy in the electric field can be identified with proper spin-wave modeling.

II. EXPERIMENTAL DETAILS

Figure 1(a) shows the schematic structure of the 65-nm-diameter MTJ device. The stack consisted of a PtMn (15 nm)/$Co_{70}Fe_{30}$ (2.6 nm)/Ru (0.86 nm)/$Co_{12}Fe_{72}B_{16}$ (2.8 nm)/MgO barrier (1.2 nm)/$Co_{12}Fe_{72}B_{16}$ (1.5 nm)/MgO capping (1.0 nm)/Ru (5 nm)/top electrode on a Si substrate or buffer layer. The composition of CoFeB was evaluated by an x-ray fluorescence measurement. The $Co_{70}Fe_{30}$/Ru/$Co_{12}Fe_{72}B_{16}$ layers had a synthetic ferrimagnetic structure, with the $Co_{70}Fe_{30}$ and $Co_{12}Fe_{72}B_{16}$ magnetization aligned antiparallel. For the free layer ($Co_{12}Fe_{72}B_{16}$ 1.5 nm) and using a vibrating sample magnetometer (VSM), $M_s = 1.35$ MA/m. The perpendicular saturation field was estimated as 200 mT by the VSM. From these values, the estimated surface perpendicular magnetic anisotropy (K_s) of the free layer was 1.5 mJ/m^2. The electric field effect in MgO-based MTJ was caused by purely electronic effects as reported in our previous work [7,8]. To maximize the electric field modulation in A_{ex}, 65-nm-diameter MTJ devices and a 1.5-nm-thick free layer were utilized. The ferromagnetic layer thickness employed here was the thinnest

possible for the MTJ with a certain MR ratio, providing a reliable frequency shift in the spectrum. To avoid spin-transfer torque and/or thermal effects, we chose $\sim 125\ \Omega\,\mu m^2$ resistance-area products for the devices.

The measurement geometry is shown in Fig. 1(b) [19,20]. H_{ext} was applied in the direction perpendicular to the sample. The measurements were performed at fixed frequencies from 1.0–6.5 GHz and a sweeping H_{ext} from 400–0 mT with a bias voltage ranging from −0.65 to 0.65 V. The critical current is the limit value for fluctuation divergence and the occurrence of steady-state precession, and was determined as 5.7×10^{10} A/m^2. This value is much larger than the applied current densities [$(0.9–4.3) \times 10^9$ A/m^2] in the MTJ. The regions of the applied current densities were near equilibrium states, far from any transition [21]. Therefore, the spin-wave excitation source was the thermal energy at room temperature [22]. We repeated measurements in three different devices (MTJ1, MTJ2, and MTJ3). All devices essentially provided the same results.

III. RESULTS AND DISCUSSION

Figure 1(c) shows a typical TE FMR spectrum observed for the MTJ. The spectrum was obtained at a microwave frequency of 6.0 GHz as a function of H_{ext} under a dc bias of 0.52 V. A positive voltage is defined as a voltage that accumulates electrons in the free layer. The open black circles are experimental results and the red line is the Lorentzian fit result. By comparison with our previous study [20], all resonance peaks belonged to the lowest nodal circle mode, i.e., $n = 1$, because of the very small size of the magnetic cell. The nodal radius mode indices l are indicated on top of the peaks. The highest intensity peak is the fundamental peak, i.e., the $n = 1$ and $l = 0$ mode. The next two peaks appearing at ∼175 mT are $l = \pm 1$ peaks. The smallest peaks at ∼130 mT are $l = \pm 2$ modes, as indicated in Fig. 1(c). In Fig. 1(d), schematic diagrams for each mode are shown. As previously mentioned, exchange splitting occurs between $l = 0$, 1, and 2, while dipole splitting occurs between the $\pm l$ modes [20].

The H_{ext} dependence of the mode frequency of MTJ1 is shown in Fig. 2(a). The peaks were measured under a bias voltage of 0.52 V. The H_{ext} dependence of the resonance peaks is almost straight and all modes are parallel to each other. The slope provides the gyromagnetic ratio $\gamma = -2\pi \times 28.3$ GHz/T for the fundamental mode $(n, l) = (1, 0)$. This is typical behavior for perpendicularly magnetized films [20].

The bias-voltage dependence of MTJ1, represented as the frequency shift of the resonance peak under a fixed H_{ext} of 200 mT, is plotted in Fig. 2(b). For each plot, the corresponding mode index is shown in the same graph. Voltage effects on the resonance frequency are clearly observed. As observed in previous work, the voltage effect is not always linear, and a biquadratic component may appear [10]. Therefore, in Fig. 2(b), the experimental points are fitted using quadratic functions.

Micromagnetic simulations were performed to estimate the sensitivity of the resonance frequencies for a small change in A_{ex}, i.e., df/dA_{ex}, by using the object-oriented micromagnetic framework (OOMMF) [23] and superimposed a sinc function to investigate FMR simulations [24]. We selected a disk shape with dimensions of 65 nm × 65 nm × 1.5 nm with a cell size of 1 nm × 1 nm × 1.5 nm for the CoFeB free layer of the nanomagnet at zero temperature. A more detailed simulation method can be found in our previous results [20].

In Figs. 3(a)–3(c), the parameter dependence of the resonance frequency under 200 mT of H_{ext} for each mode is shown. A higher A_{ex} provides more exchange splitting, as shown in Fig. 3(a). A higher K_s increases the perpendicular anisotropy field and resonance frequencies. A higher M_s causes a large demagnetization field and a decrease in the resonance frequencies. For the calculations of Figs. 3(a) and 3(b), M_s value as 1.35 MA/m is employed. K_s is determined by reproducing the experimentally obtained $l = 0$ mode frequencies in the simulations. The determined value was $K_s = 1.40$ mJ/m^2, less than that obtained in the experimental evaluations ($K_s = 1.5$ mJ/m^2). The origin of the deviation may be a particular property of the magnetic disk, such as a damaged or dull edge, that was not considered in the simulations. Finally, A_{ex} was found to be 3.25 pJ/m by fitting the size of the exchange splitting between different nodal radius modes. Owing to the MgO capping layer in our film, the residual concentration of B may be higher than that of other experiments [25,26]. In addition, in a very thin $Co_{12}Fe_{72}B_{16}$ (1.5 nm) film, a small distribution in the film thickness may cause a substantial reduction of the atomic bond lengths between ferromagnetic atoms, causing a significant reduction in A_{ex}.

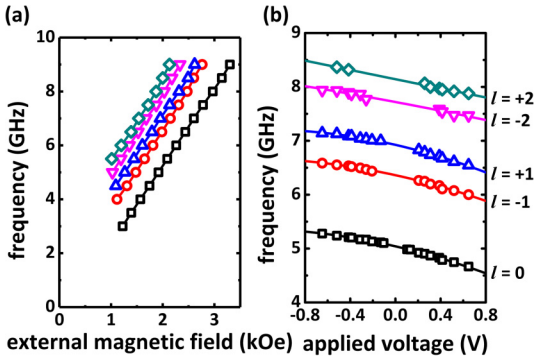

FIG. 2. (a) External field dependence of the eigenfrequency for each mode under a bias of 0.52 V. (b) Voltage dependence of eigenmode frequencies at H_{ext} at 200 mT. The nodal radius mode indices are written at the side of the graph. The lines represent least squares fitting curves using a quadratic function.

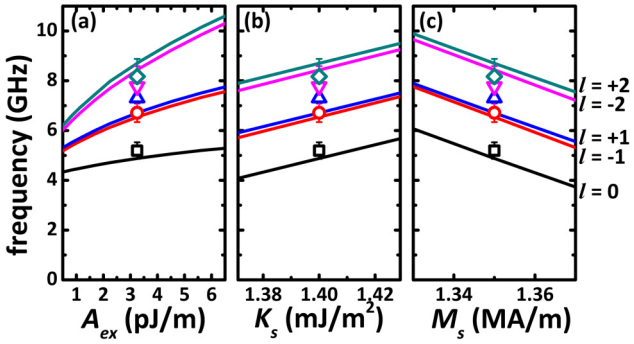

FIG. 3. Micromagnetic simulation results (lines) and experimental results (symbols) with errors for $H_{\rm ext} = 200$ mT and zero bias voltage. (a) $A_{\rm ex}$ dependent spin-wave frequencies at fixed K_s and M_s. (b) K_s dependent spin-wave frequencies at fixed $A_{\rm ex}$ and M_s. (c) M_s dependent spin-wave frequencies at fixed $A_{\rm ex}$ and K_s.

From Fig. 3, we also obtained the slope of the eigenfrequencies as a function of each parameter. In Fig. 4(a), the mode dependence of $\partial f_l/\partial A_{\rm ex}$, $\partial f_l/\partial K_s$, and $\partial f_l/\partial M_s$ is shown. As shown in the figure, $\partial f_l/\partial K_s$ and $\partial f_l/\partial M_s$ are almost independent of the mode indices, particularly for $l = 1$ and 2. Conversely, $\partial f_l/\partial A_{\rm ex}$ shows a strong mode dependence. Therefore, if the experimentally obtained voltage dependence of the resonance frequency shows a clear l-mode dependence, there is strong evidence for the modulation of $A_{\rm ex}$ by the voltage application. The simple perturbation theory for spin waves semiquantitatively agrees with the simulation results (see Supplemental Material [27]) and provides physical meaning of those slopes.

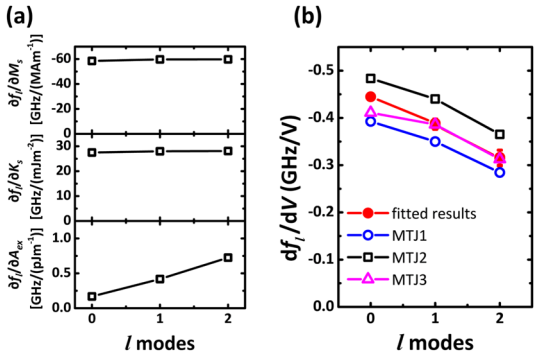

FIG. 4. (a) Slope of the spin-wave eigenfrequencies as a function of M_s (top panel), K_s (center panel), and $A_{\rm ex}$ (bottom panel) calculated from the micromagnetics. The black open rectangles represent the average values of the $\pm l$ modes. (b) Representation of df_l/dV from the experimental and fitted results as a function of each l mode. The open black rectangles, blue circles, and magenta triangles represent the experimental results of the average values of the ± 1 mode with standard deviations of the whole measured device. The red filled circles are the fitted results with errors.

In Fig. 4(b), the experimentally obtained voltage dependence of the resonance frequency is shown for different l modes, shown by the open symbols. The value of the experimentally obtained df_l/dV (blue open circles) was calculated from the slope of the fitting curve in Fig. 2(b) at a zero bias voltage. The other two experimentally obtained df_l/dV values were calculated using the same method. To simplify the analysis, averages of the $l = \pm 1$ and $l = \pm 2$ modes were obtained. A clear l-mode dependence undoubtedly reveals the existence of the modulation of $A_{\rm ex}$ by the voltage, as discussed previously. For simplicity, we assumed $\partial f_l/\partial K_s$ and $\partial f_l/\partial M_s$ were constant for the $l = 1$ and 2 modes and estimated $dA_{\rm ex}/dV$ as follows,

$$\frac{dA_{\rm ex}}{dV} = \frac{\left.\frac{df_1}{dV}\right|_{\rm expt} - \left.\frac{df_2}{dV}\right|_{\rm expt}}{\left.\frac{\partial f_1}{\partial A_{\rm ex}}\right|_{\rm sim} - \left.\frac{\partial f_2}{\partial A_{\rm ex}}\right|_{\rm sim}} = 0.23 \pm 0.02\,{\rm pJ/V\,m}. \quad (1)$$

This corresponds to an 8.6% change in $A_{\rm ex}$ for the application of 1 V. By assuming a 1.2-nm-thick MgO barrier, the electric field derivative of $A_{\rm ex}$ is $0.28 \pm 0.03 \times 10^{-21}$ J/V. The fitted results are shown in Fig. 4(b) (red circles).

In general, the voltage modulation of the resonance frequency, $(df_l/dV)dV$, may originate from the voltage modulation of $A_{\rm ex}$, K_s, and M_s. Such a contribution can be approximated using the following linear expansion:

$$\frac{df_l}{dV} = \frac{dA_{\rm ex}}{dV}\frac{\partial f_l}{\partial A_{\rm ex}} + \frac{dK_s}{dV}\frac{\partial f_l}{\partial K_s} + \frac{dM_s}{dV}\frac{\partial f_l}{\partial M_s}, \quad l = 0, \pm 1, \pm 2. \quad (2)$$

Through use of the experimentally obtained voltage modulation of the eigenfrequencies for five independent eigenmodes, i.e., $df_l/dV|_{\rm expt}$, $l = 0$, ± 1, ± 2, and the numerically obtained 15 modulation coefficients, $\partial f_l/\partial A_{\rm ex}|_{\rm sim}$, $\partial f_l/\partial K_s|_{\rm sim}$, $\partial f_l/\partial M_s|_{\rm sim}$, $l = 0, \pm 1, \pm 2$, we obtain the three unknown voltage coefficients, i.e., $\partial f_l/\partial A_{\rm ex}$, $\partial f_l/\partial K_s$, and $\partial f_l/\partial M_s$ through a least-squares method. The results are summarized in Table I by employing the electric field derivative representation ($d_{\rm MgO} = 1.2$ nm). The general least-squares method provided a similar value of $dA_{\rm ex}/dE$, i.e., $0.30 \pm 0.04 \times 10^{-21}$ J/V. In addition, the analysis provided the size of the voltage control of the magnetic anisotropy (VCMA); $dK_s/dE = -60 \pm 24$ fJ/V m. The obtained value of VCMA was a reasonable value for the system. Typical values are of a few tens of fJ/V m [28]. dM_s/dE was also evaluated but was negligible so we will not comment further.

In Table I, the electric field modulation values of $A_{\rm ex}$ determined from the domain-size observation [13,14] are

TABLE I. Experimentally and theoretically obtained values of the electric-field-induced magnetic parameters. The data include the FMR measurements using $l = 1$ and 2 modes and all peaks (this work), maze domain size (Refs. [11] and [12]), and *ab initio* calculations (ref. [10]).

	Method	dA_{ex}/dE $[10^{-21}$ (J/m)/ (V/m)]	dA_{ex}/dE (%)	dA_{ex}/dE for 1ML $[10^{-21}$ (J/m)/ (V/m)]	dK_s/dE [(fJ/m^2)/(V/m)]	dM_s/dE [(mA/m)/ (V/m)]	Reference
$Co_{12}Fe_{72}B_{16}$ 1.5 nm (65 nm MTJ)	FMR ($l = 1, 2$)	0.28 ± 0.03	8.6	≈ 2.8	-	-	This work
$Co_{12}Fe_{72}B_{16}$ 1.5 nm (65 nm MTJ)	FMR (all peaks)	0.26 ± 0.04	8.1	≈ 2.6	-60 ± 24	-0.018 ± 0.012	This work
Co 0.27 nm near T_C	Maze domain size	0.12	100	≈ 0.16	27	0.26	Ando *et al.* [13]
$Co_{40}Fe_{40}B_{20}$ 1.5 nm (1 mm junction)	Maze domain size	-1.4	-15	≈ -15	-82	0.11	Dohi *et al.* [14]
Co 1 ML/Pt (111)	*Ab initio* calculation	0.70	1.9	0.70	-114	-	Oba *et al.* [12]

also listed together with a theoretical prediction [12]. A positive electric field (depression of electrons at the surface) significantly enhances the exchange interaction, except for in the case reported by Dohi *et al.* [14]. The determination of the exchange modulation from the domain-size observation may be difficult as all modulations, i.e., $\partial f_l/\partial A_{ex}$, $\partial f_l/\partial K_s$, and $\partial f_l/\partial M_s$ affect the domain size. The separation of the exchange modulation requires independent measurements of the other contributions. Conversely, in our experiments the modulation of A_{ex} can be clearly distinguished from the K_s and M_s modulations, as was explained previously. Therefore, dA_{ex}/dV data could be could obtained that allow direct comparison with first-principle theories. In Table I, an 8.6% electric field modulation of A_{ex} under a 1 V/nm electric field for the 1.5-nm $Co_{12}Fe_{72}B_{16}$ film was obtained in the experiments. If this is a surface effect, then an 85% modulation is possible for a 1 atomic layer $Co_{12}Fe_{72}B_{16}$ film, as was shown in Ando's experiments [13]. The impact of the electric field effect on the exchange interaction may be significant.

We will now briefly discuss the mechanism of the electric-field-induced A_{ex} changes. Theoretically, Takahashi *et al.* reported the relationship between the number of d electrons and T_C, which behaves like the Slater-Pauling curve for the $3d$ magnetic alloy [29], where the increase in valence d electrons causes an increase in T_C for Fe-rich Fe-Co alloys, and vice versa for Co-rich Fe-Co alloys. For Fe-rich alloys, electron doping of 0.01 electrons to 1 atom results in a T_C increase of $\sim$17 K. This represents $\sim$1% of T_C. Therefore, an electron doping of 1% is required to modulate A_{ex} by 1%. For Co-rich Fe-Co alloys, electron doping of 0.01 electrons to 1 atom results in a T_C decrease of $\sim$4 K. Therefore, an electron doping of 1% is required to modulate A_{ex} by -0.25%. The composition of our sample is Co:Fe = 14:86. Therefore, an enhancement of A_{ex} due to electron doping is expected.

The charge doping per unit cell in the Fe interface can be expressed as

$$Q = CV = \varepsilon_0 \varepsilon_r \frac{S}{d} V, \tag{3}$$

where C is the capacitance of the MgO barrier, V is the applied voltage, ε_0 (ε_r) is the permittivity of free space (dielectric constant), S is the surface area, and d is the thickness of MgO. In our system, a variation of ± 0.03 electrons per ferromagnetic atom on the surface of the $Co_{12}Fe_{72}B_{16}$ layer can be produced by applying ± 1 V. If those electrons are doped in the d shell, applying $+1$ V may cause a 0.3% increase in A_{ex} of the surface magnetic layer [29] by considering the free-layer thickness [$\sim$10 monolayers (ML)]. In contrast, we observed a change greater than 9% for 1 V. This change is 30 times greater than that expected from the discussion based on the Slater-Pauling curve.

Oba *et al.* calculated a 1.9% increase in A_{ex} for 1 ML Co when 1 V is applied [12]. This is greater than that expected from the Slater-Pauling curve and opposite in sign. The difference in sign was explained by the shielding of the electric field, owing to the *sp* electrons and the decreased number of d electrons that are present when *sp* electrons accumulate. The large number of electric field modulations in A_{ex} from the calculations was discussed, with mention of the *sp-d* hybridization and pseudogaps appearing

in the spin-spiral states. However, the mechanism was not clearly explained in the paper. Although the theory predicts an enhancement in the electric field modulation in A_{ex}, our observations provided an even larger modulation. To understand this, further analysis using first-principle calculations and analytic models are required.

IV. CONCLUSION

In conclusion, the electric-field-induced A_{ex} changes in a 65-nm-diameter $Co_{12}Fe_{72}B_{16}$ nanomagnet were observed using TE FMR measurements. The electric field dependence of the spin-wave eigenfrequencies showed a different electric field change for different radius nodal modes. Such properties made it possible to independently evaluate the electric field dependence of A_{ex}. The analysis provided an electric field modulation in A_{ex} of $0.26 \pm 0.04 \times 10^{-21}$ J/V for the 1.5 nm $Co_{12}Fe_{72}B_{16}$ film. This corresponded to an 8.1% change in A_{ex} under a 1 V/nm electric field. The effect is useful for controlling the domain size, T_C, and other magnetic properties by the application of an electric field.

ACKNOWLEDGMENTS

This work was partially supported by the ImPACT Program through the Council for Science, Technology, and Innovation, Cabinet Office, Government of Japan. J. C. was supported by the Postdoctoral Fellowship for Foreign Researchers program (No. P16362) of the Japan Society for the Promotion of Science (JSPS). The work is also partially supported by the "Materials research by Information Integration" Initiative (MI^2I) of the NIMS, National Research Foundation (NRF) of Korea (Grant No. 2015M3D1A1070465), DGIST R&D Program of the Ministry of Science, ICT, and Future Planning (Grant No. 17-BT-02).

[1] M. Weisheit, S. Fähler, A. Marty, Y. Souche, C. Poinsignon, and D. Givord, Electric field-induced modification of magnetism in thin-film ferromagnets, Science **315**, 349 (2007).

[2] T. Maruyama, Y. Shiota, T. Nozaki, K. Ohta, N. Toda, M. Mizuguchi, A. A. Tulapurkar, T. Shinjo, M. Shiraishi, S. Mizukami, Y. Ando, and Y. Suzuki, Large voltage-induced magnetic anisotropy change in a few atomic layers of iron, Nat. Nanotechnol. **4**, 158 (2009).

[3] T. Nozaki, Y. Shiota, S. Miwa, S. Murakami, F. Bonell, S. Ishibashi, H. Kubota, K. Yakushiji, T. Saruya, A. Fukushima, S. Yuasa, T. Shinjo, and Y. Suzuki, Electric-field-induced ferromagnetic resonance excitation in an ultrathin ferromagnetic metal layer, Nat. Phys. **8**, 491 (2012).

[4] Y. Shiota, T. Nozaki, F. Bonell, S. Murakami, T. Shinjo, and Y. Suzuki, Induction of coherent magnetization switching in a few atomic layers of FeCo using voltage pulses, Nat. Mater. **11**, 39 (2012).

[5] K. Tanaka, S. Miwa, Y. Shiota, N. Mizuochi, T. Shinjo, and Y. Suzuki, Large voltage-induced magnetic anisotropy field change in ferrimagnetic FeGd, Appl. Phys. Expr. **8**, 073007 (2015).

[6] S. Kanai, Y. Nakatani, M. Yamanouchi, S. Ikeda, H. Sato, F. Matsukura, and H. Ohno, Magnetization switching in a CoFeB/MgO magnetic tunnel junction by combining spin-transfer torque and electric field-effect, Appl. Phys. Lett. **104**, 212406 (2014).

[7] S. Miwa, K. Matsuda, K. Tanaka, Y. Kotani, M. Goto, T. Nakamura, and Y. Suzuki, Voltage-controlled magnetic anisotropy in Fe|MgO tunnel junctions studied by x-ray absorption spectroscopy, Appl. Phys. Lett. **107**, 162402 (2015).

[8] T. Kawabe, K. Yoshikawa, M. Tsujikawa, T. Tsukahara, K. Nawaoka, Y. Kotani, K. Toyoki, M. Goto, M. Suzuki, T. Nakamura, M. Shirai, Y. Suzuki, and S. Miwa, Electric-field-induced changes of magnetic moments and magnetocrystalline anisotropy in ultrathin cobalt films, Phys. Rev. B **96**, 220412 (R) (2017).

[9] S. Miwa, M. Suzuki, M. Tsujikawa, K. Matsuda, T. Nozaki, K. Tanaka, T. Tsukahara, K. Nawaoka, M. Goto, Y. Kotani, T. Ohkubo, F. Bonell, E. Tamura, K. Hono, T. Nakamura, M. Shirai, S. Yuasa, and Y. Suzuki, Voltage controlled interfacial magnetism through platinum orbits, Nat. Commun. **8**, 15848 (2017).

[10] T. Nozaki, A. Kozioł-Rachwał, W. Skowronski, V. Zayets, Y. Shiota, S. Tamaru, H. Kubota, A. Fukushima, S. Yuasa, and Y. Suzuki, Large Voltage-Induced Changes in the Perpendicular Magnetic Anisotropy of an MgO-Based Tunnel Junction with an Ultrathin Fe Layer, Phys. Rev. Appl. **5**, 044006 (2016).

[11] D. Chiba, S. Fukami, K. Shimamura, N. Ishiwata, K. Kobayashi, and T. Ono, Electric-field control of magnetic domain-wall velocity in ultrathin cobalt with perpendicular magnetization, Nat. Mater. **10**, 853 (2011).

[12] M. Oba, K. Nakamura, T. Akiyama, T. Ito, M. Weinert, and A. J. Freeman, Electric-Field-Induced Modification of the Magnon Energy, Exchange Interaction, and Curie Temperature of Transition-Metal Thin Films, Phys. Rev. Lett. **114**, 107202 (2015).

[13] F. Ando, H. Kakizakai, T. Koyama, K. Yamada, M. Kawaguchi, S. Kim, K.-J. Kim, T. Moriyama, D. Chiba, and T. Ono, Modulation of the magnetic domain size induced by an electric field, Appl. Phys. Lett., **109**, 022401 (2016).

[14] T. Dohi, S. Kanai, A. Okada, F. Matsukura, and H. Ohno, Electric-field effect on spin-wave resonance in a nanoscale CoFeB/MgO magnetic tunnel junction, AIP Adv. **6**, 075017 (2016).

[15] K. Nawaoka, S. Miwa, Y. Shiota, N. Mizuochi, and Y. Suzuki, Voltage induction of interfacial Dzyaloshinskii–Moriya interaction in Au/Fe/MgO artificial multilayer, Appl. Phys. Expr. **8**, 063004 (2015), and private communication

[16] Y. Nakatani, M. Hayashi, S. Kanai, S. Fukami, and H. Ohno, Electric field control of Skyrmions in magnetic nanodisks, Appl. Phys Lett. **108**, 152403 (2016).

[17] P.-J. Hsu, A. Kubetzka, A. Finco, N. Romming, K. von Bergmann, and R. Wiesendanger, Electric-field-driven switching of individualmagnetic skyrmions, Nat. Nanotechnol. **12**, 123 (2017).

[18] M. Schott, A. Bernand-Mantel, L. Ranno, S. Pizzini, J. Vogel, H. Béa, C. Baraduc, S. Auffret, G. Gaudin, and D. Givord, The skyrmion switch: Turning magnetic skyrmion bubbles on and off with an electric field, Nano Lett. **17**, 3006 (2017).

[19] S. Tamaru, H. Kubota, K. Yakushiji, M. Konoto, T. Nozaki, A. Fukushima, H. Imamura, T. Taniguchi, H. Arai, S. Tsunegi, S. Yuasa, and Y. Suzuki, Observations of thermally excited ferromagnetic resonance on spin torque oscillators having a perpendicularly magnetized free layer, J. Appl. Phys. **115**, 17C740 (2014).

[20] J. Cho, S. Miwa, K. Yakushiji, S. Tamaru, H. Kubota, A. Fukushima, S. Fujimoto, E. Tamura, C.-Y. You, S. Yuasa, and Y. Suzuki, Spin-wave eigenmodes in single disk-shaped FeB nanomagnet, Phys. Rev. B **94**, 184411 (2016).

[21] S. Petit, C. Baraduc, C. Thirion, U. Ebels, Y. Liu, M. Li, P. Wang, and B. Dieny, Spin-Torque Influence on the High-Frequency Magnetization Fluctuations in Magnetic Tunnel Junctions, Phys. Rev. Lett. **98**, 077203 (2007).

[22] W. F. Brown, Jr. Thermal fluctuations of a single-domain particle, Phys. Rev. **130**, 1677 (1953).

[23] M. J. Donahue, and D. G. Porter, OOMMF User's Guide Version 1.0. Interagency Report NISTIR 6376 (National Institute of Standards and Technology 1999).

[24] K.-S. Lee, D.-S. Han, and S.-K. Kim, Physical Origin and Generic Control of Magnonic Band Gaps of Dipole-Exchange Spin Waves in Width-Modulated Nanostrip Waveguides, Phys. Rev. Lett. **102**, 127202 (2009).

[25] J. Cho, J. Jung, S.-Y. Cho, and C.-Y. You, Effect of annealing temperature on exchange stiffness of CoFeB thin films, J. Magn. Magn. Mater. **395**, 18 (2015).

[26] J. Cho, J. Jung, K.-E. Kim, S.-Y. Park, M.-H. Jung, and C.-Y. You, Effects of sputtering Ar gas pressure in the exchange stiffness constant of $Co_{40}Fe_{40}B_{20}$ thin films, J. Magn. Magn. Mater. 339, 36 (2013).

[27] See Supplemental Material at https://link.aps.org/ supplemental/10.1103/PhysRevApplied.10.014033 about an analytic solution for the parameter dependence of the mode frequencies.

[28] W. Skowroński, T. Nozaki, D. D. Lam, Y. Shiota, K. Yakushiji, H. Kubota, A. Fukushima, S. Yuasa, and Y. Suzuki, Underlayer material influence on electric-field controlled perpendicular magnetic anisotropy in CoFeB/MgO magnetic tunnel junctions, Phys. Rev. B **91**, 184410 (2015).

[29] C. Takahashi, M. Ogura and H. Akai, First-principles calculation of the Curie temperature Slater–Pauling curve, J. Phys.: Condens. Matter **19**, 365233 (2007).